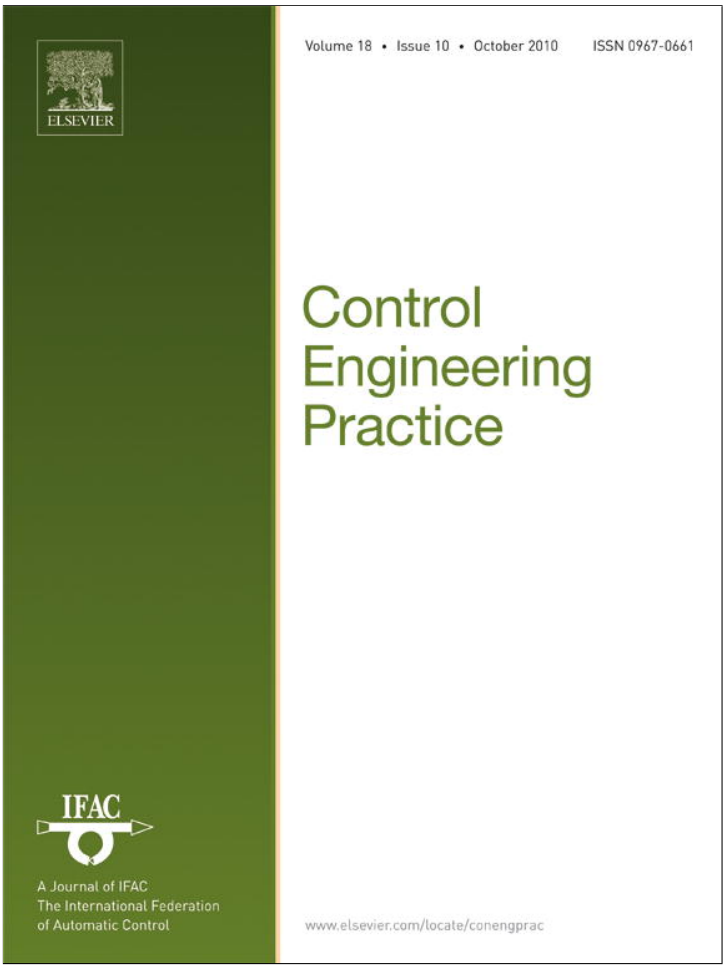

Control Engineering Practice 18 (2010) 1121–1132

Contents lists available at ScienceDirect

Control Engineering Practice

journal homepage: www.elsevier.com/locate/conengprac

Dynamic positioning systems: An experimental analysis of sliding mode control

E.A. Tannuri [a,*], A.C. Agostinho [a], H.M. Morishita [b], L. Moratelli Jr[b]

[a] Mechatronics Engineering Department, Escola Politécnica, University of São Paulo, Av. Prof. Mello Moraes, 2231, CEP 05508-030 Cidade Universitária, São Paulo, SP, Brazil
[b] Naval Architecture and Ocean Engineering Department, Escola Politécnica, University of São Paulo, Av. Prof. Mello Moraes, 2231, CEP 05508-030 Cidade Universitária, São Paulo, SP, Brazil

ARTICLE INFO

Article history:
Received 4 April 2009
Accepted 18 June 2010
Available online 16 July 2010

Keywords:
Sliding mode control
Marine systems
Nonlinear control
Robust control
PID controllers

ABSTRACT

Vessel dynamic positioning (DP) systems are based on conventional PID-type controllers and an extended Kalman filter. However, they present a difficult tuning procedure, and the closed-loop performance varies with environmental or loading conditions since the dynamics of the vessel are eminently nonlinear. Gain scheduling is normally used to address the nonlinearity of the system. To overcome these problems, a sliding mode control was evaluated. This controller is robust to variations in environmental and loading conditions, it maintains performance and stability for a large range of conditions, and presents an easy tuning methodology. The performance of the controller was evaluated numerically and experimentally in order to address its effectiveness. The results are compared with those obtained from conventional PID controller.

1. Introduction

A dynamic positioning system (DPS) is defined as a set of components used to keep a floating vessel at a specific position or to follow a pre-defined path by means of propeller action. Several offshore operations use DPSs, such as drilling, underwater pipe-laying, offloading, and diving support (Fossen, 1994).

A DPS is a complex system composed of several sensors, control and filtering algorithms, and propellers. The sensors are used to measure the position of the floating vessel, while the algorithms are responsible for calculating the forces to be delivered by each propeller to counteract environmental forces, such as wind, waves, and current loads. A simplified block diagram of a DPS is presented in Fig. 1, in which the connections between the wave filter, wind filter, controller, thruster allocation algorithm, propeller, and vessel are shown. It is a normal feedback control system with wind feed-forward action with two additional blocks: the first is a wave filter that suppresses the high-frequency motion from the measurements, and the second is a thrust allocation algorithm that is necessary to distribute the forces among the propellers as a DPS vessel is generally over-actuated.

The number of vessels with DPSs has increased in recent years due to increased oil and gas exploration at sea. In Brazil, as well as offshore operations, such as drilling, diving support, and anchor handling, DPSs have been increasingly applied to shuttle tankers during offloading operation with FPSO (floating production storage and offloading).

Commercially, DPSs are based on an extended Kalman filter (EKF) and conventional controllers (proportional derivative, PD). Integral action is provided by the compensation of estimated low-frequency external forces. The estimation of such forces is performed by the EKF. This control architecture was first proposed by Balchen, Jenssen, and Saelid (1976), and a real scale validation was later presented by Balchen, Jenssen, and Saelid (1980). This proposal has been modified, as presented in Saelid, Jenssen, and Balchen (1983). They proposed a new frequency adaptation algorithm to improve the performance of the system under a wider range of environmental conditions. Grimble, Patton, and Wise (1980) performed an extensive analysis of the Kalman filter by comparing it to the notch filter used previously in DP systems. Next, Fung and Grimble (1983) proposed a self-tuning algorithm to automatically adjust the Kalman filter matrixes, with good results. Despite improvements in the filter and estimation algorithms, the controller was still based on optimal control theory.

However, there are some problems related to the application of a linear PD controller to the DPS. Gain adjustment is a very complicated task which requires time-consuming tests at sea during the DPS commissioning. Moreover, the controller's performance varies with the environmental and loading conditions, which is not desirable as some DP operations take up to 30 h, for example offloading operations. The DP operator must manually alter the controller gains according to the environmental

* Corresponding author. Tel./fax: +55 11 30915414.
E-mail address: eduat@usp.br (E.A. Tannuri).

0967-0661/$ - see front matter © 2010 Elsevier Ltd. All rights reserved.
doi:10.1016/j.conengprac.2010.06.007

Nomenclature

A_F and A_L wind frontal and lateral projected areas [m^2]
$B(\eta)$ matrix relating the influence of thruster forces on the system state
C_{XW}, C_{YW}, and C_{NW} wind coefficients
$\boldsymbol{f}(\boldsymbol{\eta},\dot{\boldsymbol{\eta}})$ functions that define the dynamics of the system
f_R non-modeled resonant frequency [Hz]
f_S sampling rate [Hz]
$F_i(\cdot)$ maximum modeling error of functions $\boldsymbol{f}(\boldsymbol{\eta},\dot{\boldsymbol{\eta}})$
F_{1E}, F_{2E}, and F_{6E} environmental forces and yaw moment, [N] or [N m]
F_{1T}, F_{2T}, and F_{6T} thrusters total forces and yaw moment [N] or [N m]
F_{1W}, F_{2W}, and F_{6W} wind forces and yaw moment [N] or [N m]
I_Z moment of inertia of the vessel about the vertical axis [kg m^2]
$\boldsymbol{I}_\lambda$ diagonal matrix defined by the parameters λ_i
$\boldsymbol{J}(\psi)$ coordinate transformation matrix
$\boldsymbol{K}$ vector with components $k_i\text{sat}(s_i/\Phi_i)$
k_i control parameter related to the switching term
L vessel length [m]
M vessel displacement [kg]
$\boldsymbol{M}$ vessel mass matrix
M_{11}, M_{22}, M_{66}, and M_{26} surge [kg], sway [kg], yaw [kg m^2], and sway–yaw [kg m] added masses
$OXYZ$ earth-fixed reference frame
$O'x_1x_2x_6$ body-fixed reference frame
V wind velocity [m/s]
$\boldsymbol{s}(\boldsymbol{\eta},\dot{\boldsymbol{\eta}})$ vector with variables s_i that define the sliding surface $S(t)$
$S(t)$ sliding surface
t time [s]
t_{reach} time for the system trajectory to reach the sliding surface $S(t)$ [s]
T draft [m]
T_A time delay [s]
$x_1(.)$, $x_2(.)$, and $x_6(.)$ mid-ship surge, sway, and yaw absolute position [m] or [rad]
$\dot{x}_1(.)$, $\dot{x}_2(.)$, and $\dot{x}_6(.)$ mid-ship surge, sway, and yaw absolute velocities [m/s] or [rad/s]
$\ddot{x}_1(.)$, $\ddot{x}_2(.)$, and $\ddot{x}_6(.)$ mid-ship surge, sway, and yaw absolute acceleration [m/s^2] or [rad/s^2]
x_G longitudinal position of the center of mass of the vessel relative to the mid-ship section [m]
X,Y, and ψ position and heading at the point O' related to the earth-fixed reference frame [m] or [rad]
$\dot{X}$, $\dot{Y}$, and $\dot{\psi}$ velocities at the point O' related to the earth-fixed reference frames [m/s] or [rad/s]
$\ddot{X}$, $\ddot{Y}$, and $\ddot{\psi}$ acceleration at the point O' related to the earth-fixed reference frames [m/s^2] or [rad/s^2]
X_D,Y_D, and ψ_D desired position and heading (set-points) [m] or [rad]

Greek letters

ρ_a air density [kg/m^3]
Φ_i control parameters related to the boundary layer
β_W wind incidence angle relative to $ox1$ [rad]
δ_i control parameters related to the convergence velocity
η vector of vessel horizontal position and heading [m and rad]
η_d vector of desired vessel horizontal position and heading [m and rad]
ν vector of vector of mid-ship velocities relative to the body-fixed frame [m/s and rad/s]
λ_i control parameters related to the system bandwidth

Special symbols

1 (subscripts) relative to surge motion
2 (subscripts) relative to sway motion
6 (subscripts) relative to yaw motion
E (subscripts) relative to environmental agents
T (subscripts) relative to propulsion system
$\hat{}$ (on the variable) estimated value
$\sim$ (on the variable) error—difference between real and desired values

conditions. Furthermore, internal automatic gain scheduling is used to adjust the control gains when the loading condition of the vessel changes. Finally, the nonlinearity of the model, related to the heading angle, demands adjustments of the control parameters for different angles (normally in steps of 15°).

Another important issue is the robustness of the controller. The mathematical model used to describe the vessel's motion at sea, where the vessel is subjected to wind, currents, and waves, is highly nonlinear, and some phenomena are difficult to model mathematically. Thus, the DPS control's design must consider the property of robustness. Performance and stability must be guaranteed for dynamic models, similar to (but not the same as) those of the nominal model used for the controller's design. Robustness issues were initially considered using a linear approach in DPS design in the 1990s. Several authors, including Katebi, Grimble, and Zhang (1997), Nakamura and Kajiwara (1997), Tannuri and Donha (2000), and Donha and Tannuri (2001), applied the H_∞ methodology. The controller presented satisfactory robustness properties, with good performance in the presence of large variations in environmental conditions, modeling errors, and parameter uncertainty. However, it is a linear controller, which is based on a linear model of the system. Thus, different controllers must be designed with several points defined in the state-space that are close to points that the vessel reaches during operation. A "gain-scheduling" approach should then be used (Yoerger, Newman, & Slotine, 1986). However, stability cannot be ensured by conventional techniques, and numerical simulation-based methods must be used to ensure stability (Pait & Kassab, 2001). Nguyen and Sørensen (2009) proposed a hybrid DP system with supervisory switching control logic to alternate between the bank of controllers and observers. Unlike a conventional gain-scheduling approach, there are structural differences among the controllers, and different control logics can be used for a range of calm to harsh environmental conditions. The authors demonstrated the stability of the system and presented an experimental validation.

Nonlinear controllers have been applied to DPS to overcome linearization problems as they do not require switching controllers. Fossen and Strand (1998), Fossen and Grovlen (1998), Aarset, Strand, and Fossen (1998), and Zakartchouk Jr. and Morishita (2009) applied nonlinear back stepping controllers with very good results. Some difficulties in the parameters tuning

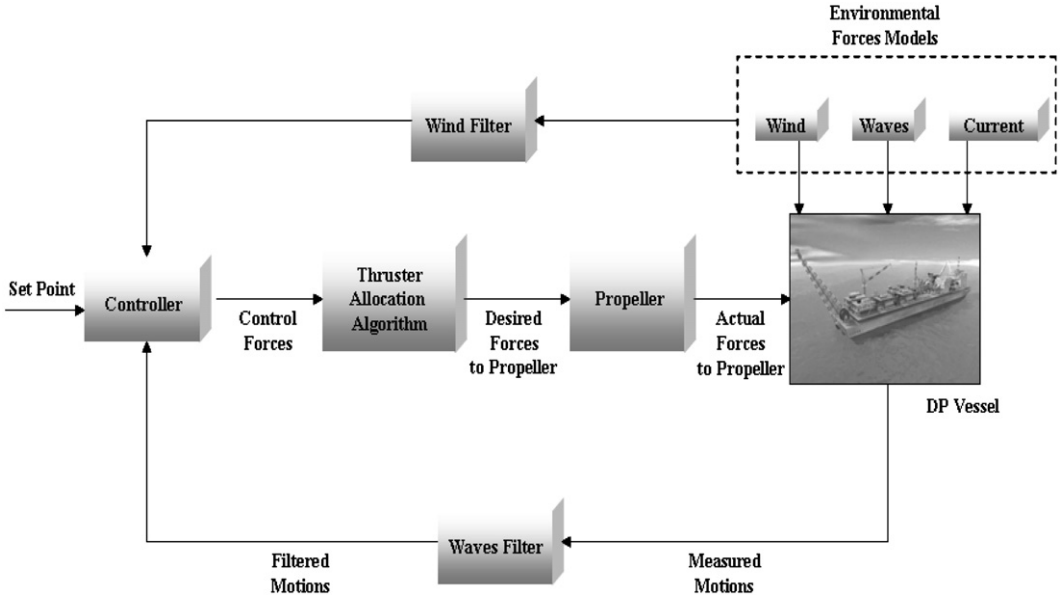

Fig. 1. DP system block diagram.

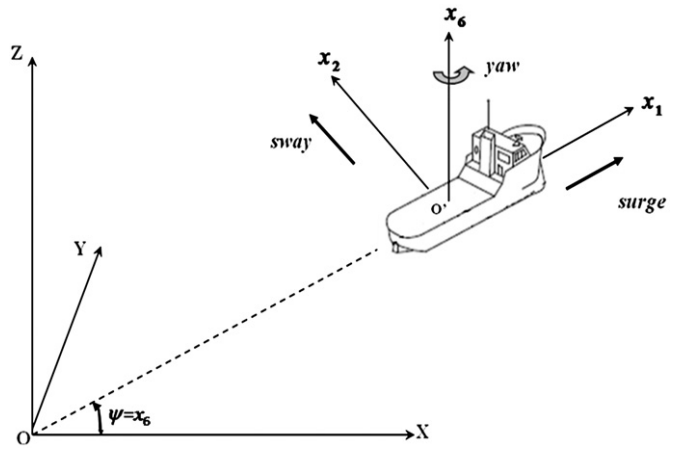

Fig. 2. Coordinate systems.

were also verified. Nonlinear control theory has also been applied to other problems related to vessel motion control, such as rudder-roll stabilization (O'Brien, 2009).

Tannuri, Donha, and Pesce (2001) applied nonlinear sliding mode control (SMC) theory to DPSs. simulations to demonstrate the robust properties of the controller. Furthermore, a simple and intuitive control tuning process was used. This control methodology was also successfully applied to several nonlinear mechanical systems, such as robotic manipulator (Slotine, 1985), positioning systems for underwater remote operated vehicles (ROVs) (Yoerger et al., 1986), vessel track control (Papoulias & Healey, 1992), and roll stabilization (Koshkouei, Burnham, & Law, 2007).

The purpose of this paper is to present the experimental validation of a control algorithm based on the robust and nonlinear SMC theory. The nonlinear controller approach ensures achievement of the performance and stability requirements for all heading angles. Because the controller contains vessel model information, an estimated mass is used as a parameter; furthermore, the same performance is ensured for different loading conditions without requiring a gain-scheduling approach. SMC only contains nine parameters, which can be easily adjusted with simple equations. The controller can be applied in a large range of environmental conditions, without performance degradation in severe conditions and for loading variations. The performance of the controller was evaluated through tests with a scale model of a tanker in the towing tank at the Department of Naval Architecture and Ocean Engineering at the University of São Paulo.

This paper is organized as follows: the mathematical modeling of the system is described in the second section. In the third section, the sliding mode control technique theory is presented. In the fourth section, the procedure to adjust the SMC parameters is described. Finally, the experimental set-up and results are presented, including comparisons between the SMC and PID controller. Extreme conditions are also used to evaluate the robustness of the proposed controller.

2. Mathematical modeling

In this section, the mathematical model of the horizontal dynamics of a floating vessel with three degrees of freedom (DOF) is presented. Ship's DPS are only concerned with low-frequency horizontal vessel motions (surge, sway, and yaw). The natural period of vertical motions are normally in the range of 5–15 s, outside the bandwidth of the positioning controller, and are excited by first-order wave forces. The wave filter is then responsible for the attenuation of such components in the positioning signals that are fed-back to the positioning controller. It must be noted that semi-submersibles may present a dynamic coupling between low-frequency horizontal and vertical motions (due to the large natural periods of vertical motions). In this case, a different design approach may be used (Sørensen & Strand, 2000).

2.1. Equations of motion

The vessel's low-frequency motions are expressed in two separate coordinate systems (Fig. 2). The inertial system fixed to the earth is indicated by *OXYZ* and the vessel-fixed non-inertial reference frame is indicated by $O'x_1x_2x_6$. The origin O' for the latter system is the intersection of the mid-ship section with the ship's longitudinal plane of symmetry. The axes for this system

coincide with the principal axes of inertia of the vessel with respect to the origin. The motions along the axes $O'x_1$, $O'x_2$ and the rotation around the $O'x_6$ are called surge, sway, and yaw, respectively.

The mathematical model that describes the low-frequency horizontal motions of the vessel, including the added mass, is given by

$$\boldsymbol{M}\dot{\boldsymbol{v}}+\boldsymbol{C}(\boldsymbol{v})\boldsymbol{v}=\boldsymbol{F_E}+\boldsymbol{F_T} \tag{1}$$

where $\boldsymbol{v}=\left[\dot{x}_1\dot{x}_2\dot{x}_6\right]^{\mathbf{T}}$ represents the vector of mid-ship velocities relative to the body-fixed frame, $\boldsymbol{F_E}=\left[F_{1E}\quad F_{2E}\quad F_{6E}\right]^{\mathbf{T}}$ is the vector of environmental forces (surge and sway) and yaw moment, $\boldsymbol{F_T}=\left[F_{1T}\quad F_{2T}\quad F_{6T}\right]^{\boldsymbol{T}}$ is the vector of thruster forces and moment and the matrixes M and C are given by

$$\boldsymbol{M}=\begin{bmatrix} M+M_{11} & 0 & 0 \\ 0 & M+M_{22} & Mx_G+M_{26} \\ 0 & Mx_G+M_{26} & I_z+M_{66} \end{bmatrix} \quad \text{and}$$

$$\boldsymbol{C}(\boldsymbol{v})=\begin{bmatrix} 0 & 0 & -(M+M_{22})\dot{x}_2+(Mx_G+M_{26})\dot{x}_6 \\ 0 & 0 & -(M+M_{11})\dot{x}_1 \\ 0 & 0 & (Mx_G+M_{26})\dot{x}_1 \end{bmatrix}$$

In those matrixes, M is the vessel mass, M_{ij} are the added masses, I_Z is the moment of inertia around the vertical axis, and x_G is the distance between vessel center of mass the O' point.

In order to design the controller, the accelerations must be isolated from (1):

$$\dot{\boldsymbol{v}}=-\boldsymbol{M}^{-1}\boldsymbol{C}(\boldsymbol{v})\boldsymbol{v}+\boldsymbol{M}^{-1}(\boldsymbol{F_E}+\boldsymbol{F_T}) \tag{2}$$

The relation between vessel coordinate system velocities (v) and the time derivative of the absolute position and heading vector $\boldsymbol{\eta}=[\eta_1\ \eta_2\ \eta_3]^{\mathbf{T}}=[X\ Y\ \psi]^{\mathbf{T}}$ is given by

$$\dot{\boldsymbol{\eta}}=\mathbf{J}(\psi)\cdot\mathbf{v};\quad \mathbf{J}(\psi)=\begin{bmatrix} \cos(\psi) & -\sin(\psi) & 0 \\ \sin(\psi) & \cos(\psi) & 0 \\ 0 & 0 & 1 \end{bmatrix} \tag{3}$$

where $\boldsymbol{J}(\Psi)$ is the coordinate transformation matrix and $\psi=x_6$.

Rewriting Eq. (2) in terms of the accelerations and velocities in the OXYZ fixed coordinate system yields the complete model of the system with three degrees of freedom:

$$\ddot{\boldsymbol{\eta}}=\boldsymbol{f}(\boldsymbol{\eta},\dot{\boldsymbol{\eta}})+\boldsymbol{B}(\boldsymbol{\eta})\boldsymbol{F_T} \tag{4}$$

where

$$\boldsymbol{B}(\boldsymbol{\eta})=\boldsymbol{J}(\psi)\boldsymbol{M}^{-1};$$

$$\boldsymbol{f}(\boldsymbol{\eta},\dot{\boldsymbol{\eta}})=\boldsymbol{g}(\dot{\boldsymbol{\eta}})-\boldsymbol{J}(\psi)\boldsymbol{M}^{-1}\boldsymbol{C}(\dot{\boldsymbol{\eta}})\boldsymbol{J}^{-1}(\psi)\dot{\boldsymbol{\eta}}+\boldsymbol{J}(\psi)\boldsymbol{M}^{-1}\boldsymbol{F_E}$$

and

$$\boldsymbol{g}(\dot{\boldsymbol{\eta}})=[-\dot{Y}\dot{\psi}\quad \dot{X}\dot{\psi}\quad 0]^{\mathbf{T}}.$$

2.2. Wind forces

The environmental forces acting on a floating vessel are due to wind, waves, and current. They are responsible for the high- and low-frequency motions of the vessel. In this paper, all tests and simulations were performed considering only the effects of wind on the vessel.

Wind forces (surge and sway) and moment (yaw) are usually defined by

$$F_{1W}=\frac{1}{2}C_{XW}(\beta_W)\rho_a A_F V^2,\quad F_{2W}=\frac{1}{2}C_{YW}(\beta_W)\rho_a A_L V^2,$$

$$F_{6W}=\frac{1}{2}C_{NW}(\beta_W)\rho_a A_L L V^2 \tag{5}$$

where F_{1W} and F_{2W} are the surge and sway components of the wind force, F_{6W} is the wind yaw moment, C_{XW}, C_{YW}, and C_{NW} are the wind coefficients, β_W is the wind incidence angle relative to the vessel, ρ_a is the air density, A_F and A_L are the frontal and lateral projected areas; L is the vessel length, and V is the wind velocity.

3. Sliding mode control

Sliding mode control is a nonlinear control methodology developed by Utkin (1978) and later modified and adapted by Slotine and Li (1991). This methodology is used to design a control law that imposes all system trajectories to converge on a surface in the space state, the so called sliding surface $S(t)$. The designer chooses the dynamics of this surface so that all trajectories will asymptotically converge to the set point. When the trajectory lies inside the sliding surface, the system operates in *sliding mode* and is insensitive to parametric variations and external disturbances. This property guarantees robustness as will be shown later.

The main disadvantage of the SMC in practical applications is the presence of a discontinuous term in the control action when the system is operating in sliding mode. It induces successive switching in the control action. This behavior tends to be more pronounced as the model uncertainties increases. This switching is called *chattering*, and can cause high-frequency oscillations around the surface $S(t)$. To eliminate the chattering, Slotine and Li (1991) suggested modifying the controller's original formulation by introducing a boundary layer around the sliding surface $S(t)$. Inside the boundary layer, the switching function is replaced by a high-gain proportional control.

The SMC design procedure consists in the definition of a sliding surface $S(t)$ (that guarantees a stable dynamic system when the trajectory lies on it) and on the selection of a control law that imposes convergence of all trajectories to the surface $S(t)$. The detailed procedure is discussed below.

Consider a MIMO (multiple input multiple output) nonlinear dynamic system given by (4), where $\boldsymbol{F_T}$ is the control input vector and the function $\boldsymbol{f}(\boldsymbol{\eta},\dot{\boldsymbol{\eta}})=[f_1\quad f_2\quad f_3]^{\mathbf{T}}$ is estimated as $\hat{\boldsymbol{f}}(\boldsymbol{\eta},\dot{\boldsymbol{\eta}})=[\hat{f}_1\quad \hat{f}_2\quad \hat{f}_3]^{\mathbf{T}}$ with an error bounded by the functions F_i:

$$|\hat{f}_i-f_i|<F_i \tag{6}$$

In the present formulation, the uncertainties associated with the matrix function $\boldsymbol{B}(\boldsymbol{\eta})$ will not be considered. It is only dependent on the mass properties of the vessel and on the heading, which are known with sufficient accuracy.

The sliding surface $S(t)$ is defined by $\boldsymbol{s}(\boldsymbol{\eta},\dot{\boldsymbol{\eta}})=0$, where $\boldsymbol{s}(\boldsymbol{\eta},\dot{\boldsymbol{\eta}})=[s_1\quad s_2\quad s_3]^{\mathbf{T}}$ is a vector composed by scalar measures of tracking errors:

$$\boldsymbol{s}(\boldsymbol{\eta},\dot{\boldsymbol{\eta}})=\dot{\tilde{\boldsymbol{\eta}}}+\boldsymbol{I}_{\boldsymbol{\lambda}}\tilde{\boldsymbol{\eta}} \tag{7}$$

where $\tilde{\boldsymbol{\eta}}=\boldsymbol{\eta}-\boldsymbol{\eta_d}$ is the tracking error associated with the pre-defined (desired) trajectory $\boldsymbol{\eta_d}=[X_d\quad Y_d\quad \psi_d]^T$, $\boldsymbol{I_\lambda}$ is the 3×3 diagonal matrix, with the principal diagonal given by the parameters $\left[\lambda_1\quad \lambda_2\quad \lambda_3\right]^T$. Those parameters are related to the closed loop bandwidth, whose value should be chosen by the designer. This implies that the sliding surface $S(t)$ should be such that $\boldsymbol{s}(\boldsymbol{\eta},\dot{\boldsymbol{\eta}})$ tends to zero as the tracking error converges to zero in finite time, i.e., $\boldsymbol{s}(\boldsymbol{\eta},\dot{\boldsymbol{\eta}})=0$, $\tilde{\boldsymbol{\eta}}=0$, and $\dot{\tilde{\boldsymbol{\eta}}}=0$. It can be shown that the relationship between $\boldsymbol{s}(\boldsymbol{\eta},\dot{\boldsymbol{\eta}})$ and the tracking error $\tilde{\boldsymbol{\eta}}$ is

defined by

$$|\tilde{\eta}_i| < \frac{\Phi_i}{\lambda_i} \tag{8}$$

where Φ_i represents the distance from the sliding surface $S(t)$ in the state-space.

To make all of the trajectories converge to $S(t)$ in a finite time t_{reach} (and to be kept there after that), a control law must be chosen that satisfies the *sliding condition* (9):

$$\frac{1}{2}\frac{d}{dt}s_i^2 \le -\delta_i|s_i|,\ \delta_i > 0 \tag{9}$$

where δ_i determines the convergence rate, whose value should be chosen by the designer. It can be shown that t_{reach} satisfies

$$t_{reach} \le \frac{|s_i(0)|}{\delta_i} \tag{10}$$

In order to satisfy the sliding condition (11) for all admissible values of $\boldsymbol{f}(\boldsymbol{\eta},\dot{\boldsymbol{\eta}})$, the control law is given by

$$\boldsymbol{F_T} = \boldsymbol{B}^{-1}(\boldsymbol{\eta})\left(-\hat{\boldsymbol{f}}(\boldsymbol{\eta},\dot{\boldsymbol{\eta}}) + \boldsymbol{\eta_R} - \boldsymbol{K}\right) \tag{11}$$

being K the vector with components $k_i\text{sat}(s_i/\Phi_i)$ and $\boldsymbol{\eta_R} = \ddot{\boldsymbol{\eta}}_{\boldsymbol{d}} - 2\boldsymbol{I}_{\boldsymbol{\lambda}}\dot{\tilde{\boldsymbol{\eta}}} - (\boldsymbol{I}_{\boldsymbol{\lambda}})^2\tilde{\boldsymbol{\eta}}$. If $k_i \ge F_i + \delta_i$, condition (9) is satisfied for all admissible values of f_i. It must be stressed that this term becomes more important as the uncertainties and disturbances increase.

The parameters k_i represent the gains of the switching terms, and Φ_i are the thicknesses of the boundary layers. The latter term is designed to compensate for the system uncertainties. The saturation function eliminates the chattering that appears in the original structure of the SMC, which uses a sign function. However, it introduces a steady state error given by (8). An integral term (with anti-windup feature) included in the definition of the variable s_i slowly eliminates such error. The saturation function is defined by

$$sat(y) = \begin{cases} y & |y| \le 1 \\ sgn(y) & |y| > 1 \end{cases}$$

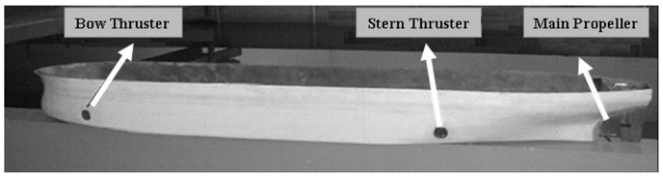

Fig. 3. Model used in the experiments.

Table 1
Vessel model properties.

	Fully loaded	Ballasted condition
Mass (M)	52.5 kg	30.5 kg
Moment inertia (I_z)	4.63 kg m^2	5.18 kg m^2
Length (L)	178 cm	
Beam (B)	29 cm	
Draft (T)	12 cm	8 cm
Surge Added Mass (M_{11})	5.25 kg	3.05 kg
Sway added mass (M_{22})	26.25 kg	15.25 kg
Yaw added mass (M_{66})	8.51 kg	4.94 kg
Sway–Yaw added mass (M_{26})	0	0
Center of mass of the vessel (x_G)	0	0

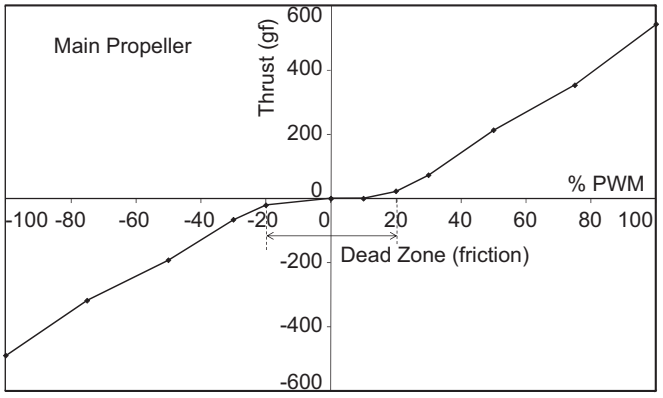

Fig. 4. Performance curve of the main propeller.

4. Sliding mode controller parameter tuning

As already mentioned, the functions $\hat{\boldsymbol{f}}(\boldsymbol{\eta},\dot{\boldsymbol{\eta}})$ correspond to the best estimate of the functions $\boldsymbol{f}(\boldsymbol{\eta},\dot{\boldsymbol{\eta}})$, depending on the mass properties of the vessel, actual position and heading, and environmental conditions. It must be stressed that a rough estimate of the environmental conditions can be used as the controller is robust to those uncertainties.

The parameters λ_i are limited by three terms: non-modeled resonant frequencies (f_R), time delay (T_A), and sampling rate (f_S), respectively, (i) $\lambda_i \le \frac{2\pi}{3}f_R$; (ii) $\lambda_i \le \frac{1}{3T_A}$; (iii) $\lambda_i \le \frac{1}{5}f_S$.

For the present problem, the adopted values are as follows:

(i) f_R is related to vertical (heave, roll and pitch) resonant modes of the vessel, that cannot be excited from the thrusters control action. For the reduced scale model (1:150) of a typical off-loading tanker used in the experiments, $f_R \cong 1\,Hz \Rightarrow \lambda_i \le 2.094$;
(ii) T_A is due to the delay induced by the low-pass wave filter. For the notch filter used in the experiments, $T_A \cong 0.8s \Rightarrow \lambda_i \le 0.417$;
(iii) f_S is 10Hz in the experiments (0.1s sampling time) $\Rightarrow \lambda_i \le 2$.

The desired control bandwidth λ_i is the minimum of the three bounds above. Therefore, the bandwidth of the closed-loop system considered was $\lambda = \lambda_1 = \lambda_2 = \lambda_3 = 0.4$.

The boundary layer thickness can be defined by Eq. (8). The maximum tracking errors in the surge, sway, and yaw adopted for the design of the controller were 0.12 m, 0.12 m, and 5°, respectively. Thus, the parameters Φ_1, Φ_2, and Φ_3 obtained were 0.05, 0.05, and 0.035, respectively.

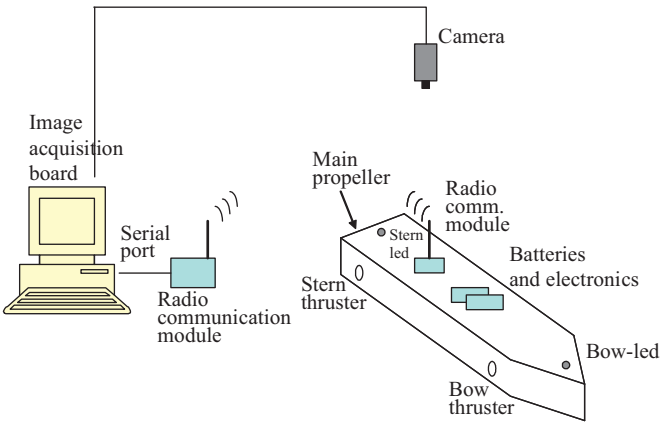

Fig. 5. Experiment arrangement.

Finally, the parameters δ_i are calculated using Eq. (10), assuming that the trajectory reaches the sliding surface in 10 s.

The gains (k_1, k_2, k_3) are calculated according to estimates of modeling error and inaccuracies in the forces and moments due to the action of environmental agents. They must satisfy the following:

$$k_i \geq \delta_i + \max\left|f_i - \hat{f}_i\right| \tag{12}$$

Tannuri et al. (2001) have described the exact formulation of the maximum errors associated with the functions f_i.

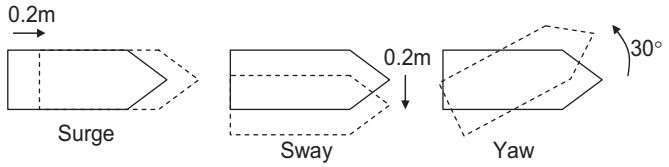

Fig. 6. Maneuvers.

5. Experimental set-up

Tests with a scale model were carried out in an academic towing tank at the Department of Naval Architecture and Ocean Engineering at the University of São Paulo to evaluate the performance of the SMC. The tank size is 1.5 m deep, 5 m wide, and 21 m long. The tests were performed with a reduced scale model (1:150) of a typical off-loading tanker. The model was equipped with a main propeller and two auxiliary thrusters, namely, the bow and stern thrusters (Fig. 3).

Table 2
Overshoot and settling time.

	Surge (X)		Sway (Y)		Yaw (ψ)	
	M_p (%)	$t_{s5\%}$ (s)	M_p (%)	$t_{s5\%}$ (s)	M_p (%)	$t_{s5\%}$ (s)
Experiment positive dir.	15	12	10	30	20	21
Experiment negative dir.	25	13	20	40	15	57
Experiment—average	20	12.5	15	35	17	39
Simulation—average	12	11	35	26	27	19

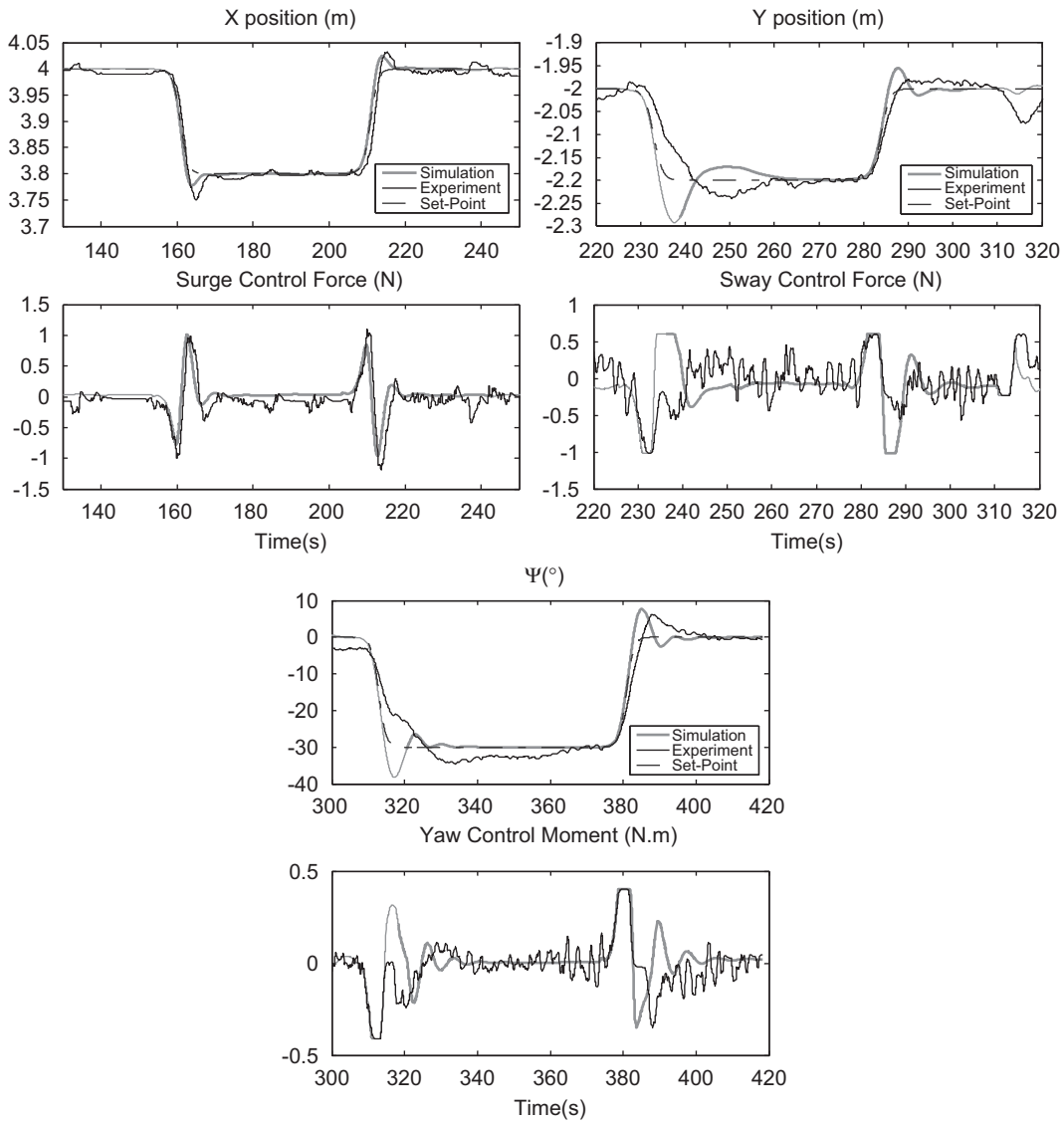

Fig. 7. Experiment and simulation (ballasted condition and no environmental action).

The main dimensions and mass properties of the vessel used in this paper under two loading conditions are given in Table 1.

Preliminary calibration was performed to determine the relationship between the thrust in each propeller and the command imposed on the motor. The motors are controlled by PWM (pulse width modulation), and the command varies from 0% to 100%. As an illustration, the curve obtained for the main propeller is shown in Fig. 4.

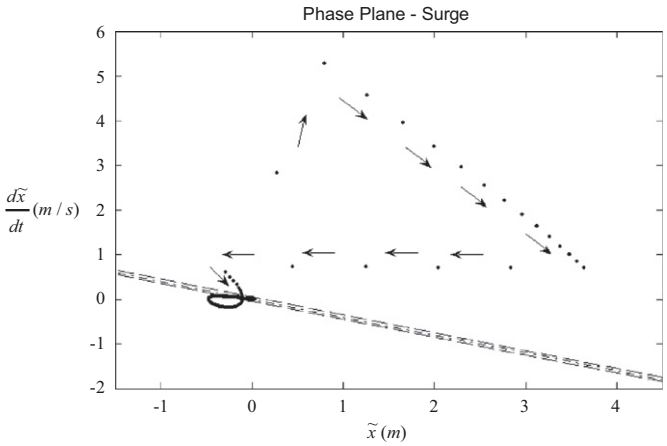

Fig. 8. Phase plane of the surge motion—simulation.

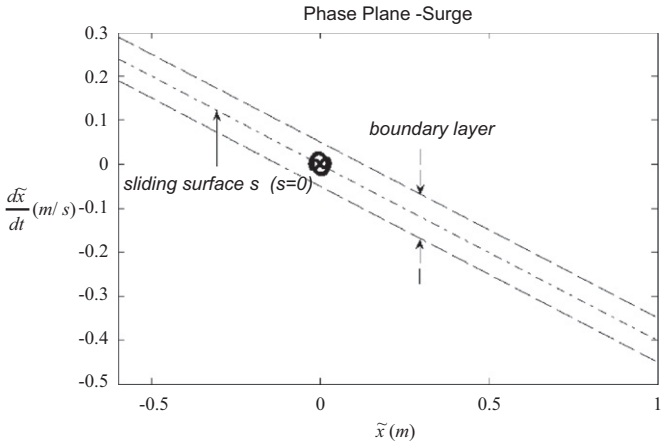

Fig. 9. Phase plane expanded—simulation.

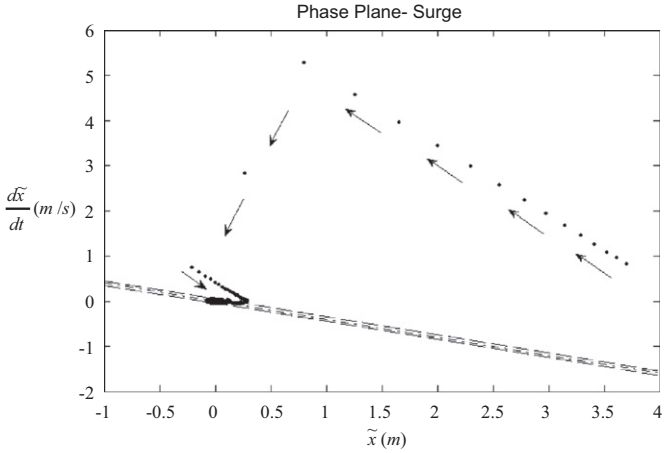

Fig. 10. Phase plane of the surge motion—test.

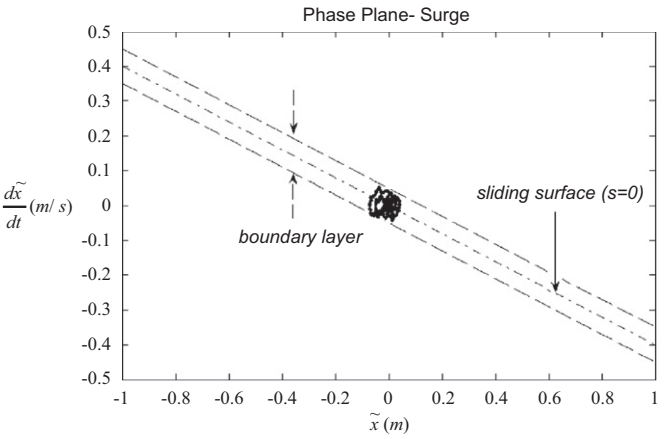

Fig. 11. Phase plane expanded—test.

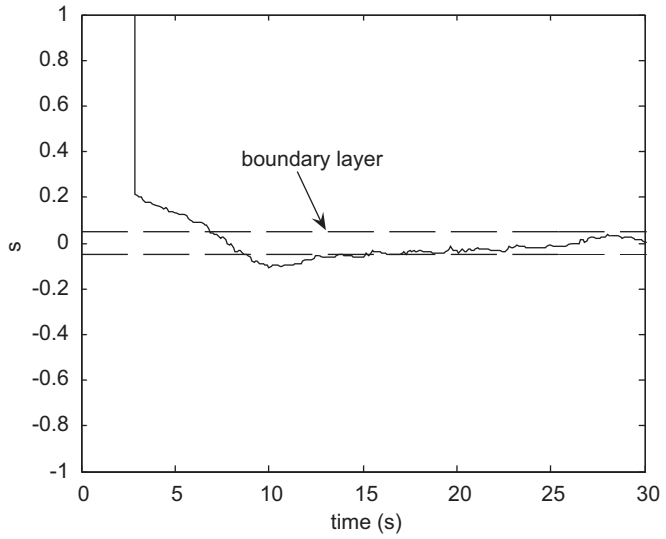

Fig. 12. Reach time (t_{reach}) and boundary layer—test.

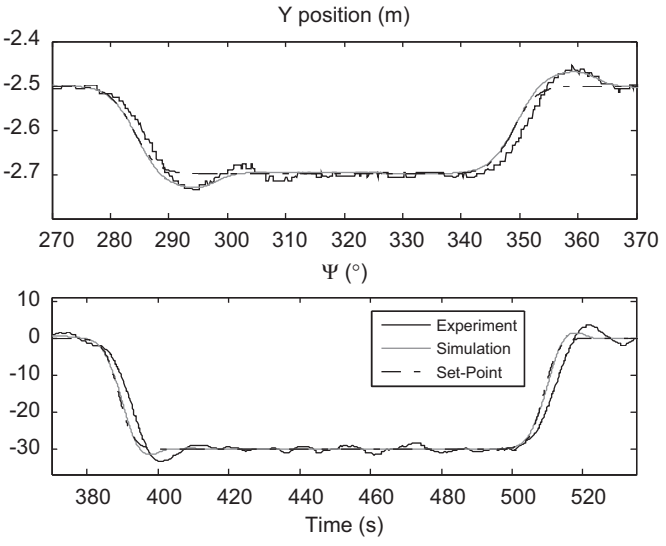

Fig. 13. Experiment and simulation (ballasted condition, no environmental action, slower set-point variation).

The dead zone is caused by friction and mechanical misalignments of the propeller parts. However, tunnel thrusters present an even larger dead zone. This fact may cause unpredictable behavior in propeller action, as the dead zone is highly sensitive to temperature, small displacements of the hull, and lubricant. The thrust delivered by the main propeller is in the range of -4.9 and $+5.4$ N, and the tunnel thrusters deliver between -0.5 and $+0.3$ N.

The position and heading measurement of the model in the tank is accomplished using an artificial vision system, which comprises of a camera and an image acquisition board. The resulting resolution of the system is approximately 10 mm. The camera captures the images of two LEDs one in the bow and one in the stern, and the system is able to determine the position and heading of the model according to an earth-fixed frame.

All numerical calculations are performed using an algorithm processed on a conventional computer, with a time-step of 0.1 s. Given the reference and the information generated by the artificial vision system, the algorithm calculates the thrust necessary to keep the model at the required position and heading. All information is sent by radio-frequency signals to a receptor onboard the model. The receptor is integrated with electronic devices which cause the propellers to work in the desired way. There is also real-time feedback in the control system with the actual rotation values. The topology of the experimental set-up is illustrated in Fig. 5. A full description of the experimental facilities is given in Tannuri and Morishita (2006).

Table 3
Overshoot and settling time—positive direction.

	Sway (Y)		Yaw (Ψ)	
	M_p (%)	$t_{s5\%}$ (s)	M_p (%)	$t_{s5\%}$ (s)
Experiment positive dir.	16	27	12	30
Experiment negative dir.	16	31	10	30
Experiment—average	16	29	11	30
Simulation—average	15	27	3	22

Table 4
Overshoot and rise time—wind action.

Wind speed (m/s)	0	1.5	2	2.5	0	1.5	2	2.5
	Rise time (s)				Overshoot (%)			
Full condition	21	21.2	21.6	21.6	11	10	13	14
Ballasted condition	19	23.4	25.5	28.2	0	0	0	0

6. Experimental results

In this paper, the performance of the SMC is experimentally evaluated through two sets of tests: set-point changes and variations in the operational condition. The former tests are intended to verify the stability and ability of the controller to work according to the specifications. The latter tests check the robustness of the SMC by changing the load of the model and environmental conditions.

6.1. Set-point changes and performance

The set-point change tests were carried out by considering maneuvers in the surge, sway, and yaw directions, as indicated in Fig. 6. A 0.2-m smooth variation was imposed on the surge set-point and returned after the stabilization. The variation of the set-point in both directions took approximately 5 s. The similar

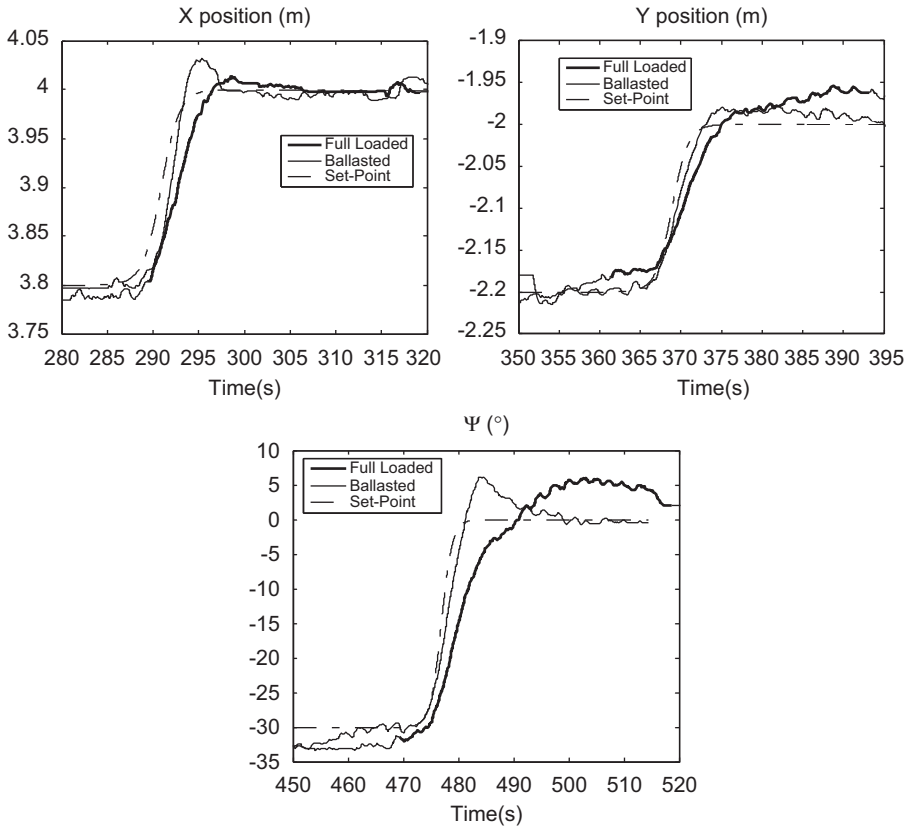

Fig. 14. Experiment in full and ballasted conditions, no environmental action.

motion was imposed in the sway direction (with a variation of 0.2 m) and in the yaw direction (with a variation angle of 30°). The load of the vessel corresponded to the ballasted condition, and no environmental agents were active over the vessel.

A low-pass filter with a cut-off frequency of 1.42 rad/s was used to filter the measured positions by the computer vision system, excluding the high-frequency noise present in this acquired signal.

Fig. 7 shows a comparison between the experimental and simulation results for the ballasted condition with no environmental action. In the surge motion, the figure shows a good overall agreement between the experimental and simulation results. However, such behavior was not observed in the sway or yaw motions. In this case, the system shows a faster response in the simulations. One possible explanation for the different performances between the simulation and experiment for the sway and yaw motions is the difference between the actual and expected behavior of the lateral thrusters, mainly after saturation. As shown in Fig. 4, the thrusters experience friction and misalignment. Such errors were not taken into account during controller design and were not considered in the simulation code.

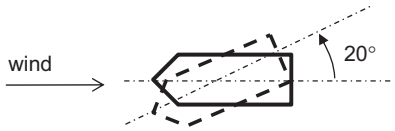

Fig. 15. Wind action—yaw maneuver.

Another reason for the difference may be the inexactness of the mathematical damping model due to the fluid–body interaction.

Table 2 shows the settling time (t_s—5% error) and overshoot (Mp) for positive and negative motion directions. As a smooth variation was applied at the set-point, the settling times were computed from the instant the set-point reached 99% of the total variation. The table also contains the average experimental values as well as the average values obtained in the simulations. The experimental results are not equal for the positive and negative directions for several reasons, these being asymmetry in the hull construction and propeller performance.

In the surge and sway motions, the settling times obtained by simulation and experiment are very similar. For the yaw motion, the settling time obtained in the negative maneuver was quite large (57 s), which resulted in an average value that was larger than that obtained in the simulation. The experimental overshoot is smaller than that obtained in the simulations for the sway and yaw maneuvers, and the opposite conclusion is drawn for the surge motion. Effects not included in the simulation code, as previously mentioned, may cause such differences.

To analyze the performance of the SMC, Fig. 8 shows the phase plane plot for the surge motion obtained by the simulation. As expected, the trajectory converges to the sliding surface ($s=0$), and once inside the boundary layer, it remains within the limits. To better visualize the trajectory within the boundary layer and the sliding surface, the phase plane is expanded and shown in Fig. 9. Fig. 10 shows the experimental phase plane of the surge motion. Fig. 11 contains a detailed view of the same phase plane. It can be seen that there are different trajectories for theoretical

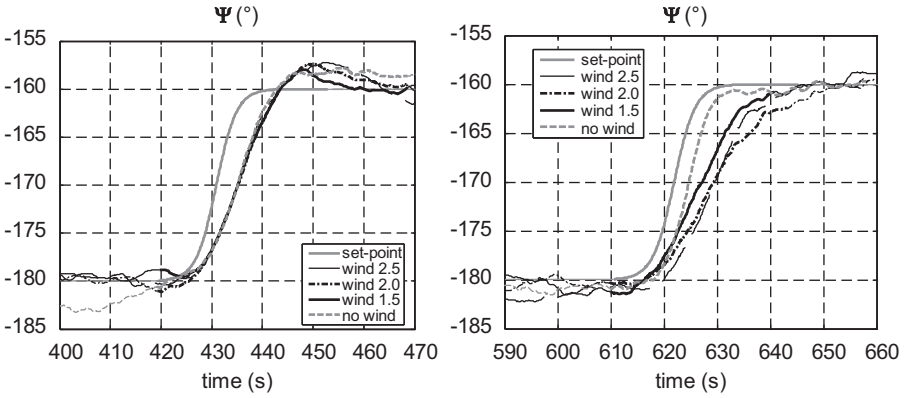

Fig. 16. Wind action—yaw maneuver full loaded condition (left), ballasted condition (right).

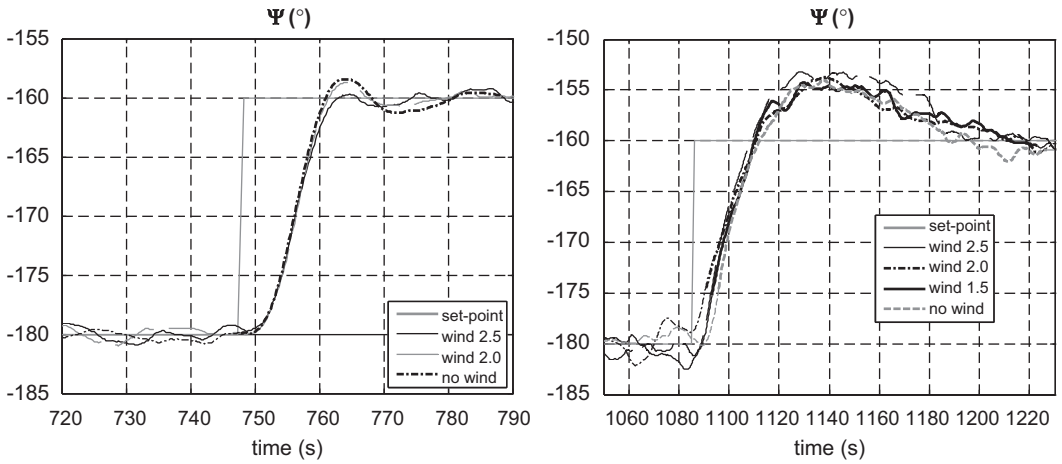

Fig. 17. Wind action—yaw maneuver, PID control (left) full loaded condition, (right) ballasted condition.

and experimental results, especially outside the boundary layer. This behavior is mainly caused by the different initial conditions used in the simulations and experiments. However, the results are similar in the sense that both trajectories tend toward the boundary layer in the first moment and then remain inside it.

To check the reach time t_{reach}, the curve of the variable s as a function of time was plotted for the experimental surge test (Fig. 12). A reach time close to 7 s is verified, which is in accordance with the design value (smaller than 10 s). Modeling errors (mainly related to the propellers, which were not considered in the controller design) explain the behavior of the s variable after the reach time. The s variable overpasses the boundary layer at $t=9$ s and returns to it at approximately $t=13$ s.

Due to the unexpected difference between the theoretical and experimental results for sway and surge, as shown in Fig. 8, a new test was carried out, varying the set-point at intervals of 10 s instead of 5 s in the sway and yaw motions. The results are shown in Fig. 13 and in Table 3, and a better agreement between the simulation and experiment can be verified, in comparison with Fig. 7. Furthermore, the settling times of the sway and yaw responses are smaller as compared to Fig. 7. The explanation for this relies on the propellers since, in the present case, no saturation is observed, and a better representation of the propellers in this non-saturated range is considered in the numerical model. It is worthwhile to verify how definition of set-point changes has an impact on the DPS performance. A reference model could be used in the generation of feasible desired trajectories and set-point changes, as proposed by Sørensen, Sagatun, and Fossen (1996).

Table 5
Overshoot and rise time—wind action, PID control.

Wind speed (m/s)	0	1.5	2	2.5	0	1.5	2	2.5
	Rise time (s)				Overshoot (%)			
Full condition	10.6		10.9	11.1	8		7	3
Ballasted condition	20	20	18	17	30	28	31	34

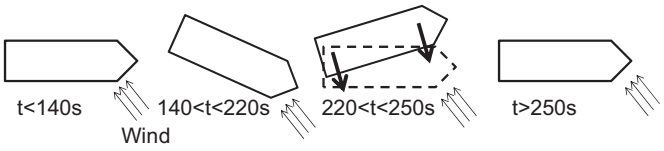

Fig. 18. First test effect of wind; steps of the maneuver.

6.2. Robustness of the controller

The most desirable characteristic of the SMC is its robustness. In this paper, it is verified through two tests: by changing the draft of the scale model and by considering external forces on it. The same control parameters used in the previous tests are considered here.

Fig. 14 shows the results for set-point changes for the surge, sway, and yaw directions with full and ballasted loaded conditions. Satisfactory performance was observed in both conditions. This illustrates the robustness of the controller. The full loaded condition presented a smaller overshoot and a slightly higher settling time because of the increase in the vessel inertia. In a real vessel, the controller must receive information regarding the actual displacement of the vessel (based on a draft monitoring system, for example). The control is then automatically adjusted for different displacements. In a conventional PID-type controller, a gain-scheduling algorithm uses the displacement of the ship, and a specific gain adjustment for each situation must be calculated during commissioning. This problem is particularly critical in the DPS applied to shuttle tankers as the displacement of such vessels increases by a factor of almost three during the offloading operation.

The robustness of the controller must be checked for variations in environmental conditions, as the mathematical model of the dynamics of the vessel is highly nonlinear. This aspect is experimentally verified in this paper by imposing different wind speeds during a heading maneuver (Fig. 15). The tests were

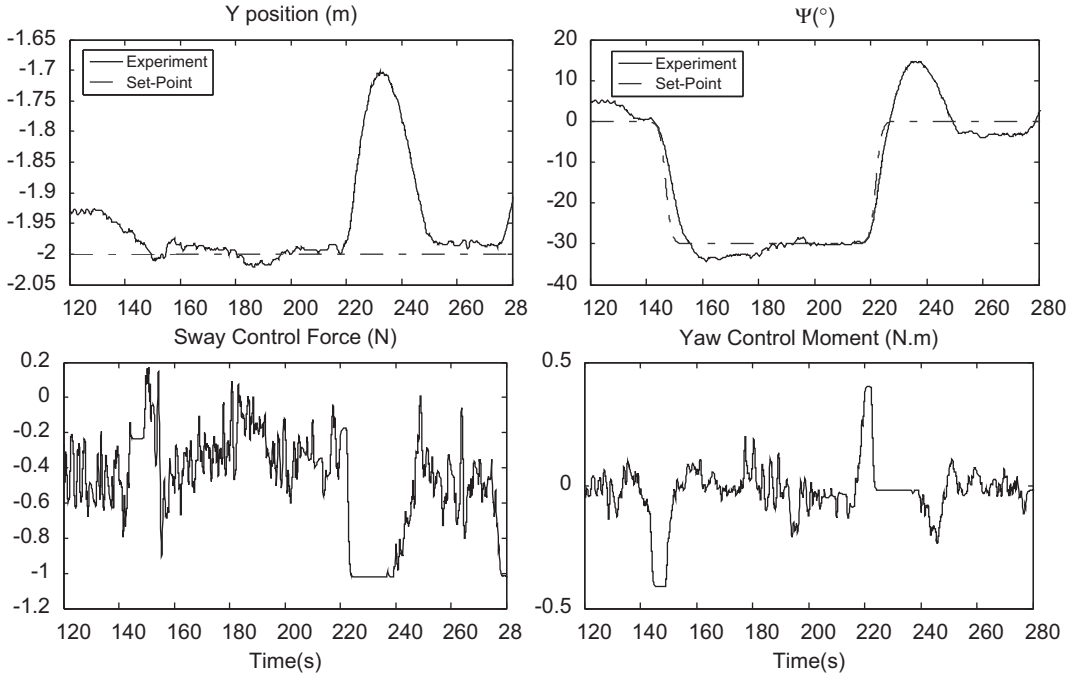

Fig. 19. Response time of the first test effect of wind.

performed in both full and ballasted condition. The results for four wind speeds are shown in Fig. 16. A Pitot tube device measured the wind speeds and the values indicated are approximate. The results reveal that in ballasted condition, wind speeds larger than 2.5 m/s caused saturation of the thrusters and position loss. The main performance parameters (overshoot, rise time) are shown in Table 4. Rise time is defined here as the time elapsed for a 15° rotation of the vessel ($-180°$ to $-165°$). It can be seen that the parameters are quite similar for each loading condition, considering all wind speeds. This result is evidence of the robustness of the controller to environmental action. It must be stressed that the same control parameters are used for both loading conditions.

The same experiment was conducted with a standard PID controller, using a gain scheduling technique to adjust the control gains for each environmental and loading condition. For the fully loaded condition, a genetic algorithm calculated PID control gains. A relay-based auto tuning technique was used for the ballasted condition. The results are shown in Fig. 17 and Table 5.

Different PID tuning procedures were used for each loading condition in order to illustrate the importance of the PID tuning method in the performance of the vessel. The genetic algorithm, used in the loaded vessel, gave a very good performance (better than SMC), with a small overshoot and rise time. On the other hand, the relay-based technique used for the ballasted condition was not satisfactory, with a large overshoot. Therefore, the results indicated that similar (or even better) performance of the vessel can be obtained with PID controller, compared to those proposed by SMC. However, such performance is dependent on the tuning procedure, and different gains must be used for each loading and environmental condition. So, the advantages of the SMC are not based on the performance itself, but on the robustness and ease of tuning.

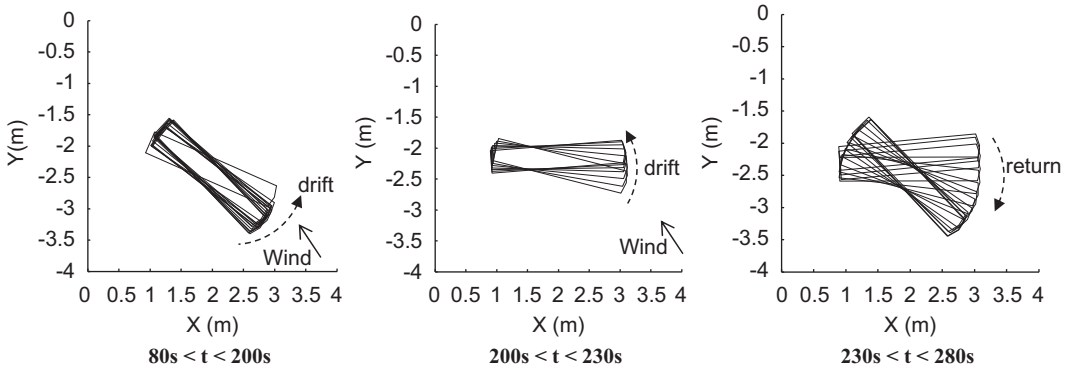

Fig. 20. Second test: effect of wind.

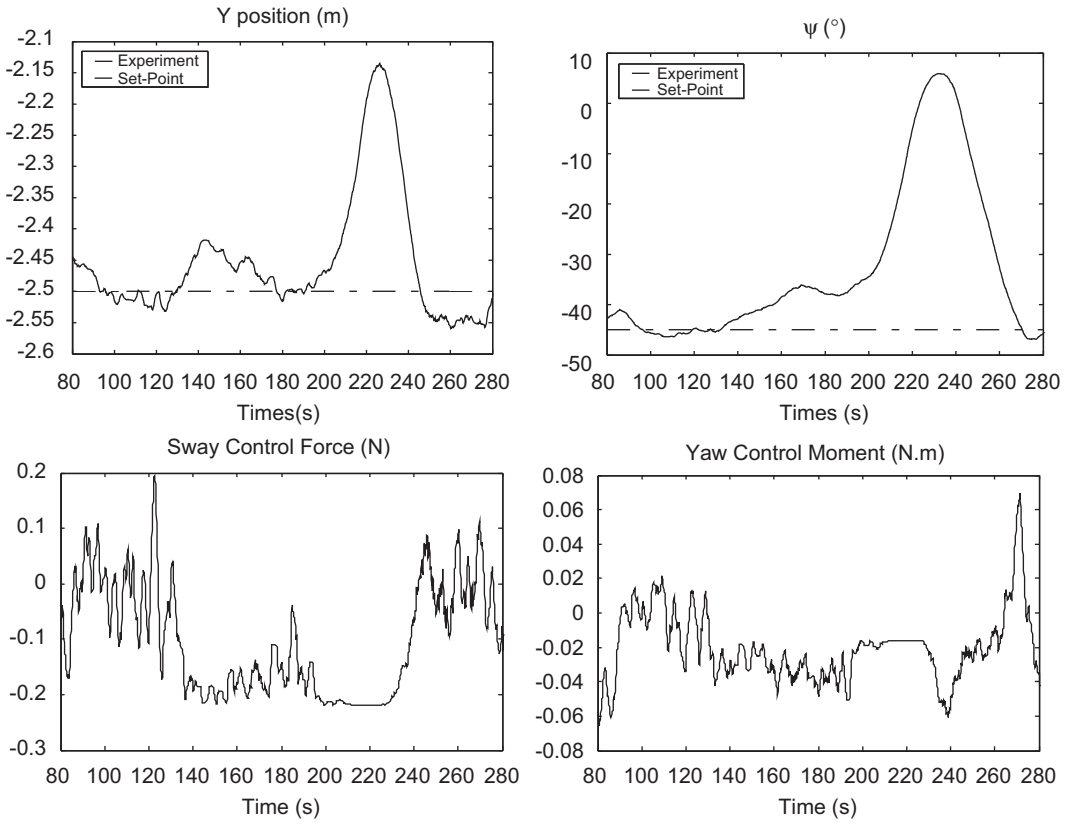

Fig. 21. Response time of the second test with wind.

To show the performance of the controller in the presence of external forces that may cause saturation of the thrusters (extreme conditions), two experiments were carried out considering a ballasted vessel under wind action. In the first experiment (wind test 1), a rotation maneuver of 30° in the yaw direction was performed heading the vessel into the wind. Next, the vessel returned to a heading of 0°. Fig. 18 shows each step of the maneuver. The wind speed was approximately 2.5 m/s.

Fig. 19 shows the time series of the sway and yaw motions and the control forces. While the vessel is heading into the wind (between 140 and 220 s), the controller does not cause saturation of the thrusters, the vessel maintains its position. During the return maneuver (at 220 s), the lateral thrusters were saturated, in order to compensate for the lateral wind. The vessel then lost position in the sway and yaw directions, with errors of 0.3 m and 15°, respectively. After 250 s, the vessel returned to the reference position. This test illustrated the good performance of the SMC in extreme conditions, even with saturation of the thrusters.

Fig. 20 shows the maneuver performed in a second experiment with wind (wind test 2), and Fig. 21 presents the corresponding time response. In this case, lower limits of saturation were imposed on the thrusters, corresponding to approximately 1/5 of the limits used in the previous experiments.

Initially, the yaw angle of the model was $-45°$ (relative to the X-axis), and the wind incidence angle was approximately 5° relative to the bow. The DP forces were saturated at certain points (between 80 and 200 s), and the vessel began to drift. Due to the thrust allocation logic being primarily intended to maintain position in the present case, the vessel lost the heading angle, which reached 35° at $t=200$ s.

After this (between 200 and 230 s), the lateral thrusters became completely saturated, and neither the heading nor the lateral position could be maintained. The model was unable to overcome the force of the wind, which caused large errors in the sway and yaw. At $t=230$ s, the wind was turned off, and the model returned to its original position. This test also illustrates the how well the controller performed (with the anti-windup feature), even in extreme situations.

7. Conclusions

This paper describes a control algorithm for dynamic positioning systems based on the sliding mode control and makes use of nonlinear multivariable mathematical models. Tuning control parameters was intuitive and easy to perform. Most of the parameters are based on physical insights. Systematic experimental tests with scale model were carried out, in order to verify control performance and robustness. The main advantage of the proposed controller, compared to the conventional PID control, is its robustness to variations in its displacement and the environmental conditions.

Acknowledgments

The authors thank Petrobras for financial support in implementing this project. The first author acknowledges the Brazilian National Research Council (CNPq), under the Processes 470999/2008-0 and 301686/2007-6. The second author thanks the Coordination for Improvement of Higher-Level Manpower (CAPES).

References

Aarset, M. F., Strand, J. P., & Fossen, T. I. (1998). Nonlinear vectorial observer backstepping with integral action and wave filtering for ships. In *Proceedings of the IFAC conference on control applications in marine systems (CAMS'98)* (pp. 83–89), Fukuoka, Japan.

Balchen, J. G., Jenssen, N. A., & Saelid, S. (1976). Dynamic positioning using Kalman filtering and optimal control theory. In *IFAC/IFIP symposium on automation in offshore oil field operation* (pp. 183–186), The Netherlands.

Balchen, J. G., Jenssen, N. A., & Saelid, S. (1980). Dynamic positioning of floating vessels based on Kalman filtering and optimal control. In *Proceedings of the 19th IEEE conference on decision and control* (pp. 852–864), USA.

Donha, D. C., & Tannuri, E. A. (2001). Non-linear semi-submersible positioning system using an H-infinity controller. In *Proceedings of the control applications in marine systems conference (IFAC-CAMS 2001)*, Glasgow, Scotland, CD-ROM.

Fossen, T. I. (1994). Guidance and control of ocean vehicles. *John Wiley and Sons, Ltd.*, 494.

Fossen, T. I., & Grovlen, A. (1998). Nonlinear output feedback control of dynamically positioned ships using vectorial observer backstepping. *IEEE Transactions on Control Systems Technology*, *6*(1), 121–128.

Fossen, T. I., & Strand, J. P. (1998). Nonlinear ship control. In *Proceedings of the control applications in marine systems conference (IFAC-CAMS'98)*.

Fung, P. T. K., & Grimble, M. J. (1983). Dynamic ship positioning using a self-tuning Kalman filter. *IEEE Transactions on Automatic Control*, *AC-28*(3), 339–350.

Grimble, M. J., Patton, R. J., & Wise, D. A. (1980). Use of Kalman filtering techniques in dynamic ship positioning. In *IEEE proceedings*, Vol. 127, Pt.D, no. 3 (pp. 93–102).

Katebi, M. R., Grimble, M. J., & Zhang, Y. (1997). $H\infty$ robust control design for dynamic ship positioning. *IEE Proceedings on Control Theory and Applications*, 110–120.

Koshkouei, A., Burnham, K., & Law, Y. (2007). A comparative study between sliding mode and proportional integrative derivative controllers for ship roll stabilization. *IET Control Theory Applications*, *1*(5), 1266–1275.

Nakamura, M., & Kajiwara, H. (1997). Control system design and model experiments on thruster assisted mooring system. In *Proceedings of the seventh international offshore and polar engineering conference (ISOPE)* (pp. 641–648), USA.

Nguyen, T. D., & Sørensen, A. J. (2009). Switching control for thruster-assisted position mooring. *Control Engineering Practice*, *17*(12), 1405–1414. December.

O'Brien, J. F. (2009). Multi-path nonlinear dynamic compensation for rudder roll stabilization. *Control Engineering Practice*, *17*(7), 985–994. September.

Pait, F. M., & Kassab, F. J. (2001). On a class of switched, robustly stable, adaptive systems. *International Journal of Adaptive Control and Signal Processing*, *15*(3), 213–238. May.

Papoulias, F. A., & Healey, A. J. (1992). Path control of surface ships using sliding modes. *Journal of Ship Research*, *36*(2), 141–153.

Saelid, S., Jenssen, N. A., & Balchen, J. G. (1983). Design and analysis of a dynamic positioning system based on Kalman filtering and optimal control. *IEEE Transactions on Automatic Control*, *AC*(3), 331–339.

Slotine, J. J. E., & Li, W. (1991). *Applied nonlinear control*. New Jersey: Prentice-Hall.

Slotine, J. J. E. (1985). The robust control of robot manipulators. *International Journal of Robotics Research*, *4*(2), 49–64.

Sørensen, A. J., Sagatun, S. I., & Fossen, T. I. (1996). Design of a dynamic positioning system using model-based control. *Control Engineering Practice*, *8*(2000), 205–213.

Sørensen, A. J., & Strand, J. P. (2000). Positioning of small-waterplane-area marine constructions with roll and pitch damping. *Control Engineering Practice*, *4*(1996), 359–368.

Tannuri, E. A., & Donha, D. C. (2000). H_∞ controller design for dynamic positioning of a turret moored FPSO. In *Proceedings of the fifth IFAC conference on manoeuvring and control of marine crafts (MCMC2000)* (pp. 269–274), Denmark.

Tannuri, E. A., & Morishita, H. M. (2006). Experimental and numerical evaluation of a typical dynamic positioning system. *Applied Ocean Research*, *28*, 133–146.

Tannuri, E. A., Donha, D. C., & Pesce, C. P. (2001). Dynamic positioning of a turred moored FPSO using sliding mode control. *International Journal of Robust and Nonlinear Control*, *11*(13).

Utkin, V. I. (1978). Sliding Modes and their application to variable structure systems. Moscow: MIR Publishers.

Yoerger, D. R., Newman, J. B., & Slotine, J. J. E. (1986). Supervisory control system for the JASON ROV. *IEEE Journal on Oceanic Engineering*, *OE-11*(3), 392–400.

Zakartchouk Jr., A., & Morishita, H. M. (2009). Backstepping controller for dynamic positioning of ships: simulation and experimental results for a shuttle tanker model. In *Proceedings of the eighth IFAC conference on manoeuvering and control of marine crafts (MCMC2009)*, Brazil.